

See discussions, stats, and author profiles for this publication at: <https://www.researchgate.net/publication/261985935>

Dislocation-Eliminating Chemical Control Method for High-Efficiency GaN-Based Light Emitting Nanostructures

ARTICLE in CRYSTAL GROWTH & DESIGN · JANUARY 2012

Impact Factor: 4.89 · DOI: 10.1021/cg2013107

CITATIONS

6

READS

51

8 AUTHORS, INCLUDING:



Young-Ho Ko

Electronics and Telecommunications Researc...

13 PUBLICATIONS 71 CITATIONS

[SEE PROFILE](#)



Suk-Min Ko

Korea Advanced Institute of Science and Tech...

17 PUBLICATIONS 84 CITATIONS

[SEE PROFILE](#)

Dislocation-Eliminating Chemical Control Method for High-Efficiency GaN-Based Light Emitting Nanostructures

Je-Hyung Kim,[†] Chung-Seok Oh,[‡] Young-Ho Ko,[†] Suk-Min Ko,[†] Ki-Yon Park,[‡] Myoungho Jeong,[§] Jeong Yong Lee,[§] and Yong-Hoon Cho^{*,†}

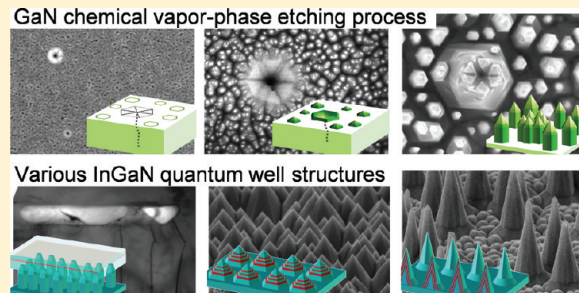
[†]Department of Physics and Graduate School of Nanoscience & Technology (WCU), Korea Advanced Institute of Science and Technology (KAIST), Daejeon, 305-701, Republic of Korea

[‡]SYSNEC Co., Ltd., 439-2, Daejeon, 305-313, Republic of Korea

[§]Department of Materials Science and Engineering, Korea Advanced Institute of Science and Technology (KAIST), Daejeon, 305-701, Republic of Korea

Supporting Information

ABSTRACT: A dislocation-eliminating chemical control method for high-quality GaN nanostructures together with various types of InGaN quantum well structures are demonstrated using a chemical vapor-phase etching technique. Unlike chemical wet etching, chemical vapor-phase etching could efficiently control the GaN and form various shapes of dislocation-free and strain-relaxed GaN nanostructures. The chemically controlled GaN nanostructures showed improved crystal quality due to the selective etching of defects and revealed various facets with reduced residual strain via the facet-selective etching mechanism. These structural properties derived excellent optical performance of the GaN nanostructures. The chemical vapor-phase etching method also showed possibilities of the fascinating applications for high-efficiency InGaN quantum well structures, such as InGaN quantum well layer on void embedded GaN layer, InGaN quantum well embedded GaN nanostructure, and InGaN/GaN core/shell nanostructure.



INTRODUCTION

Since the successful demonstration of blue light-emitting diodes based on nitride materials,¹ group-III nitrides have attracted considerable attention for research purposes and device applications^{2–5} and have led a new era of solid-state lighting. However, the growth of high-quality nitride materials still remains difficult due to the large difference in the lattice constant and thermal expansion coefficient between the nitride materials and heterosubstrates. One of the most effective ways of increasing the quantum efficiency is the formation of nanostructures (NSs), especially vertically well-aligned NSs such as nanorods and nanopyrramids. The geometrical change from an epilayer to nanorods or nanopyrramids can increase the light extraction, and the improved crystal quality of NSs can prevent the carriers from being captured by nonradiative centers, thus improving the quantum efficiency.^{6,7} However, the currently available fabrication and growth methods for NSs have their own limitations. For example, in bottom-up processes, such as the self-assembled,⁸ catalyst-driven,⁹ and selective-area growth techniques,¹⁰ despite many successful formation of GaN NSs, control and p-doping remain difficult, and contamination problems and the need for patterning process can arise. On the other hand, the top-down dry etching method offers easy and effective control of NS. However, with this method, the surface damage created by the physical etching

process limits the quantum efficiency of the NS.¹¹ Another top-down approach with chemical wet etching has advantages of negligible degradation of the crystal quality and selectivity between different materials,¹² which has been widely used for the fabrication of GaAs, ZnO, and Si-based nanostructures. Unfortunately, the great chemical stability of group-III nitrides precludes the use of chemical etchants,¹³ so common chemical wet etching techniques are not proper to form GaN NSs,^{14,15} especially on Ga-polar GaN (0001), which has a much lower surface energy than N-polar GaN (0001).¹⁶ Therefore, in spite of the high demand for high-quality NSs, the task of efficient fabricating and growing GaN NSs is met with challenges.

Here we introduce a remarkable chemical control method for the fabrication of GaN NSs. The chemical vapor-phase etching (CVE) method not only shows the effective chemical control of III-nitride materials, but also forms high-efficiency and dislocation-free NSs with improved structural and optical properties. We could control the size and shape of GaN NSs by changing the etching conditions and demonstrated some possible applications for high-efficiency InGaN quantum well (QW) structures. The facet- and defect-selective etching

Received: October 3, 2011

Revised: December 12, 2011

Published: January 25, 2012

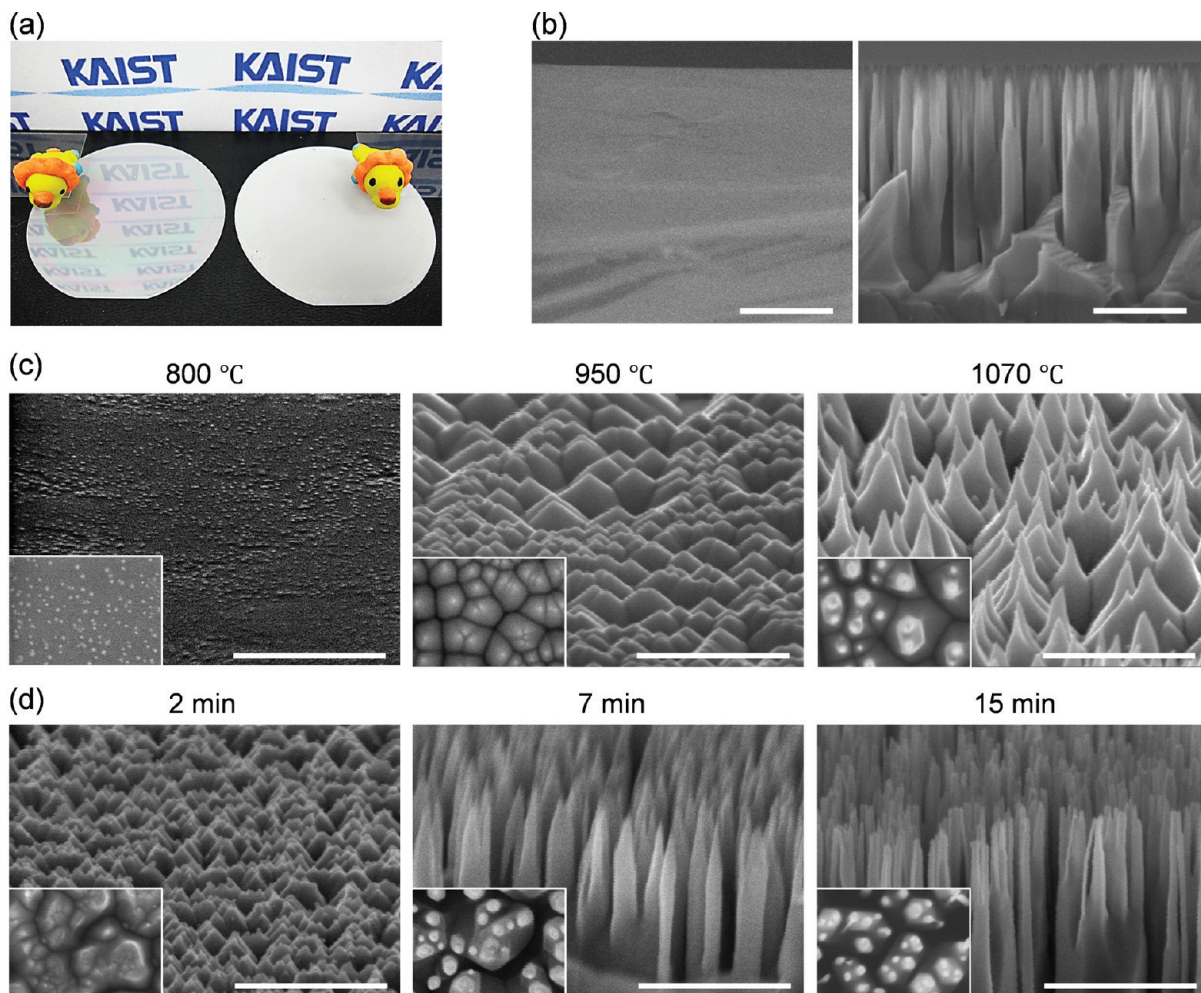


Figure 1. (a) Photographic image of the 2 in. GaN wafers before (left) and after (right) etching. (b) Cross-sectional SEM images of the GaN epilayer before etching (left) and the GaN NSs after etching (right). Scale bars = 500 nm. (c, d) Bird's eye-view SEM images of GaN NSs under different etching conditions. Inset: Plan-view SEM image. (c) Various shapes of NSs were formed at different etching temperatures: 800 °C, 950 °C, and 1070 °C. (d) Various lengths of NSs were formed at different etching times: 2 min (200 nm), 7 min (600 nm), and 15 min (1500 nm). Scale bars = 500 nm.

mechanisms play an important role in this method. These mechanisms allow a two-dimensional flat surface of the GaN epilayer to be formed into various shapes of three-dimensional NSs, such as dots, cones, and rods with high quality and high density over a large area (wafer level) and without a lithographic process.

■ EXPERIMENTAL PROCEDURES

GaN wafers with a 2 μm thickness were prepared using the metal organic chemical vapor deposition (MOCVD) (SYSNEX MARVEL 260NT) growth process including a low temperature GaN buffer layer on a *c*-plane sapphire. Six pieces of 2 in. GaN wafers grown at the same time were used for this study to eliminate the differences in each MOCVD run. The polarity of the Ga-polar GaN was confirmed through the etching of the surface using H_3PO_4 . For the chemical vapor-phase etching, we used 1000 sccm of HCl and 300 sccm of NH_3 except for the gas ratio dependent etching experiments. In addition, N_2 gas was flowed with HCl and NH_3 as a carrier gas. The temperature of the reactor was controlled at two parts; the gas mixing part and the sample substrate zone. The temperature of the gas mixing zone was fixed at 800 °C, while that of the sample substrate zone was changed depending on the experiments. The pressure of the chamber was set at 756 Torr during all the experiments. Structural characteristics of the samples were investigated using scanning electron microscopy (SEM)

(Hitachi S-4800) and 200 kV transmission electron microscopy (TEM) (JEOL JEM-2100F). The cross-sectional TEM samples were prepared by a mechanically polishing and an ion-milling process (Gatan PIPS691). For both the time-integrated photoluminescence (PL) and time-resolved PL measurements, the samples were placed in a low vibration closed-cycle cryostat that maintained stable temperatures from 5 to 300 K. A continuous-wave 325 nm He–Cd laser with an average power of 5 mW and a high sensitive photomultiplier tube (PMT) detector were used for time-integrated PL. A 350 nm frequency-doubled, mode-locked (200 fs) Ti:sapphire laser system with a peak power density of 25 MW/cm² and a time-correlated single-photon counting system with a microchannel-plate PMT was used to obtain the time-resolved PL spectra. The full width at half-maximum (fwhm) of the instrument response function of this system was less than 50 ps. The cathodoluminescence (CL) image was recorded using Mono CL4 (Gatan) coupled with SEM (Philips XL30S) at an acceleration voltage of 5 kV.

■ RESULTS AND DISCUSSION

A 2 μm thick Ga-polar GaN epilayer on a *c*-plane sapphire substrate was prepared for the CVE experiment. We exposed the GaN epilayer to vapor-phase HCl with NH_3 and N_2 gas together at a high temperature of 1070 °C, which corresponds to the growth temperature of GaN. During the CVE process,

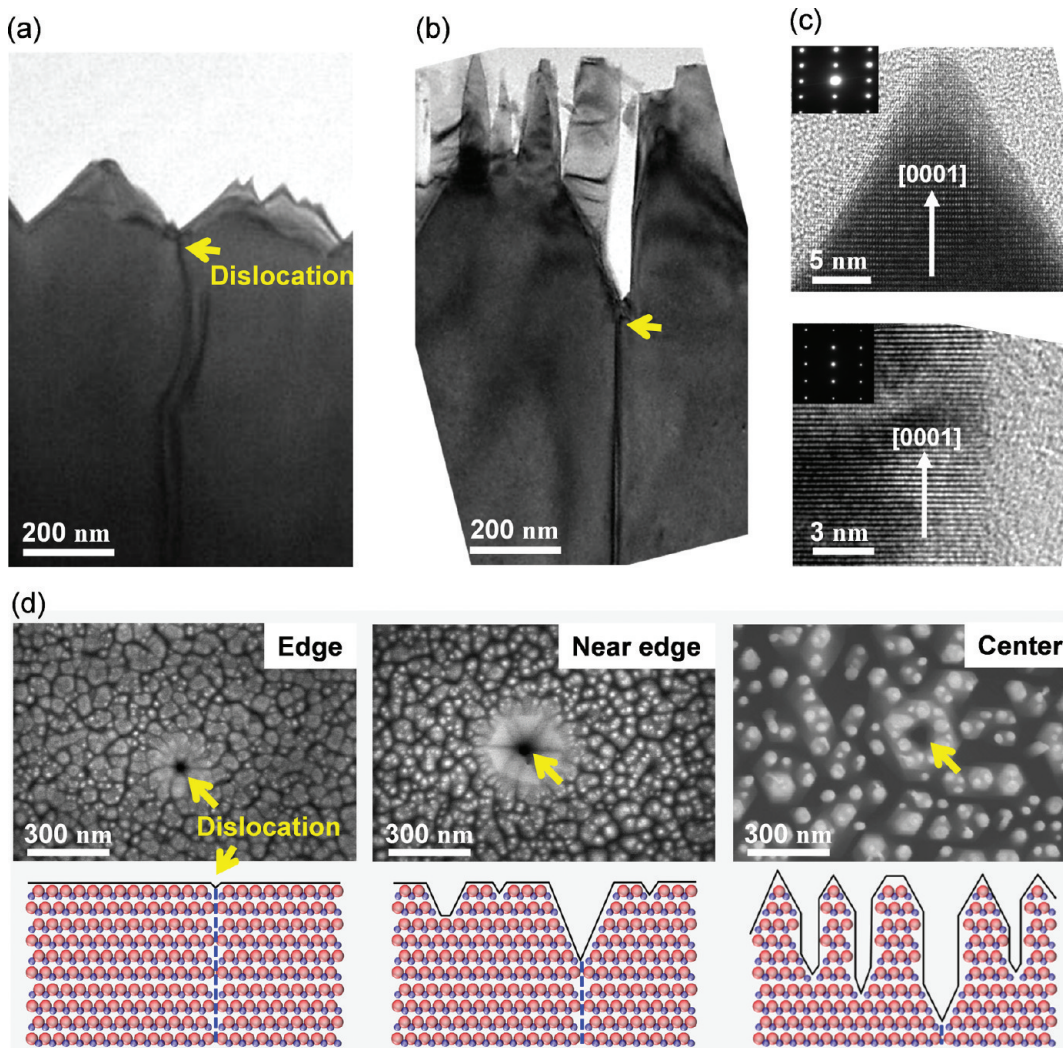
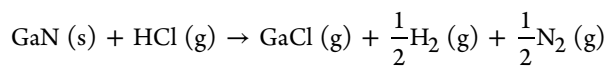


Figure 2. Cross-sectional TEM bright-field images with the samples etched at 1070 °C for (a) 2 min and (b) 7 min. The dislocations terminate between the NSs in both samples. (c) High-resolution TEM images of a single-crystalline GaN NS with a {1101} facet (upper) and a {1100} facet (lower). The insets are the electron diffraction pattern taken along the [1120] zone axis (upper) and along the [1100] zone axis (lower). (d) Plan-view SEM and cross-sectional schematic images from the edge to the center of the etched GaN wafer. The etching rate is relatively low at the edge because of the weak gas flow at the edge of the wafer. As the etching rate increases, the removal of the dislocations is clearly shown in these images. Yellow arrows indicate the dislocations.

the GaN crystal may experience the following dissociation process:^{17,18}



Although some studies on the thermodynamic and kinetic processes between GaN and HCl gas have been conducted,^{15,17,18} they did not obtain any clear NSs due to their low etching temperatures or long etching times. In our study, however, we successfully demonstrated high-quality and high-density GaN NSs on a large area via the CVE method. Figure 1a,b shows photographic images of the 2 in. GaN wafers and their cross-sectional SEM images before and after the CVE process. The mirror-like flat surface of the GaN epilayer (Figure 1a left) becomes a roughened surface showing an opaque white appearance after the etching process (Figure 1a right). The formation of vertical GaN NSs with a diameter of about 100 nm and a length of about 1.5 μm is shown in Figure 1b. The fact that the Ga-polar GaN can be effectively etched and form NSs by chemical method has great significance, because dry

etching techniques such as reactive ion etching have mostly been used to fabricate III-nitride materials even though such techniques cause severe etching damage. The chemically etched NSs are vertically well aligned and have the same horizontal level at the top position and therefore can be useful for devices fabrication such as metal deposition on the top of the NSs

To clarify how the CVE process affects the GaN, we performed several experiments under different etching conditions, such as the temperature, time, and gas ratio of HCl and NH₃. Temperature had a strong influence on the etching process because of the nature of the chemical reaction. Figure 1c shows bird's eye-view SEM images of the GaN NSs formed at different etching temperatures of 800 °C, 950 °C, and 1070 °C for 5 min. At 800 °C, the flat surface of the GaN turned into a dotted surface with a density of about 1×10^{11} cm⁻² and a height of about 7 nm. As the etching temperature was increased, the different shapes of GaN NSs were observed: a nanocone structure at 950 °C and a nanoneedle structure at 1070 °C. Similar tendency that the NSs with the vertical facets are formed at high temperature is often observed in the growth

process.^{19,20} We next changed the etching time to 2 min, 7 min, and 15 min at 1070 °C. The longer the etching time, the longer the NS we could form with a speed of approximately 100 nm/min (Figure 1d). Especially, the sample etched for 7 min (Figure 1d middle) has the shape of a nanopencil with a sharp tip. The nanopencil structure is very useful for photonic and field-emitter devices^{21,22} due to its tapered geometry for photon and electron emitting. The optical property of this sample is discussed below. We also controlled the etching gas ratio of HCl and NH₃. When we flowed only NH₃ gas without HCl gas, the GaN epilayer was not etched. Meanwhile, with HCl gas, vertical NSs were formed as a result of the etching, and the diameter of the NSs decreased with increasing the HCl gas flow (Figure S1 in the Supporting Information). Therefore, we were able to control the shape, length, and diameter of the NSs by changing the temperature, time, and etching gas ratio, respectively.

We then performed a TEM study to understand the anisotropic dissociation mechanism. Figure 2a,b shows cross-sectional TEM bright-field images of NSs etched at 1070 °C for 2 and 7 min, respectively. The high-resolution TEM images in the upper panel and lower panel of Figure 2c correspond to the GaN NSs in Figure 2a,b, respectively. The high-resolution TEM images show a smooth and clean surface of NSs without any etching damage. One interesting feature in the TEM images is that the dislocations terminate at the etched region and do not pass through the NSs, as shown in Figure 2a,b (see also Figure S2 in the Supporting Information). This observation implies that the dislocations were removed during the etching process. The removal of dislocations was confirmed again in the SEM images taken at different positions on the wafer. The plan-view SEM and cross-sectional schematic images in Figure 2d show the progress on the removal of dislocations as the etching rate increases. The formation of etch pits at the dislocation was observed at the edge of the wafer (poor etching region). Meanwhile at the main etching region (90% of the surface of the wafer), we observed the formation of NSs with the removal of the dislocations. In contrast with the high-quality crystal region, the dislocation region has crystals with an irregular atomic arrangement that increases the surface energy, causes instability, and accelerates the dissociation. Therefore, the dislocation-free GaN NSs could be obtained via the CVE method. The selective removal of dislocations reveals one of the anisotropic etching mechanisms. However, the more important mechanism for the formation of NS is the facet-selective etching due to the competition between facets that have different surface energy and etching rate. This is the most distinct difference between the chemical wet etching and the CVE. In the case of the chemical wet etching, it only forms etched pits on the surface of epilayer by the dislocation-selective etching. However, with the CVE process, it can effectively activate dissociation process in GaN, and the facet-selective etching results not only the formation of etched pits but also the formation of faceted NSs even on the dislocation-free area. The GaN NSs shows various facets depending on the etching conditions: they are mostly semipolar facets {1101} and nonpolar facets {1101}, as shown in Figure 2c. These are the facets frequently observed in the GaN NSs formed by growth techniques.²³ We can predict the faceted equilibrium shape of a NS by examining the surface energy with the growth/etching velocity of different facets. This equilibrium shape of a NS can be drawn in terms of a kinetic Wulff's plot, which is based on consideration of the surface energy and

kinetic factors.^{24,25} Figure 3 shows a schematic of a kinetic Wulff's plot and the expected equilibrium shapes for different

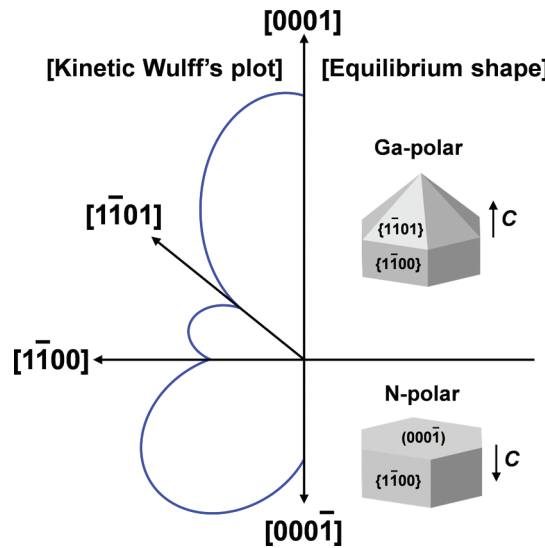


Figure 3. Schematics of a kinetic Wulff's plot on the (11-20) plane and the corresponding equilibrium shapes of the GaN NS with different polarities. The wurtzite GaN crystal with different dangling bonds of the Ga- and N-polar surface has an asymmetric equilibrium shape across the (0001) plane.

polarities under a common GaN growth condition.^{25,26} The deeper cusp in the plot means that the corresponding facet has a great chance of surviving in a competition between facets. Although the equilibrium shape of a NS can change under the influence of kinetic conditions, such as the temperature, strain, pressure and so on, many studies on experimental growth have reported that {1101} and {1101} facets can be easily found in Ga-polar GaN^{19,23,27} as shown in Figure 3. These facets are in accord with the result of the chemically etched NSs. Therefore, in the viewpoint of formation mechanism of these faceted NSs, the facet-selective etching mechanism has a similarity to the facet-selective growth mechanism and the chemical etching process can be understood in terms of a time-reversal process of growth.

We investigated the optical properties of GaN NSs, particularly the nanopencil-shaped GaN NSs shown in Figure 1d middle, and compared it with an unetched GaN epilayer as a reference by means of macro- and micro-PL, temperature-dependent PL, time-resolved PL, and CL. In the macro-PL spectra (Figure 4a), the PL peak intensity (log scale) of the GaN NS shows a 10- and 12-fold increase compared with that of the GaN epilayer at 15 and 300 K, respectively, with a peak shift toward a lower energy. The significant increase in PL intensity and the peak shift are caused by improved crystal quality and morphological changes from the epilayer to the NS,^{28,29} which enhances the light extraction and reduces the compressive stain³⁰ of the GaN. Figure 4b shows an Arrhenius plot of the normalized integrated PL intensity of the GaN NSs. The ratio of room temperature (300 K) PL intensity to low temperature (15 K) PL intensity ($I_{300\text{ K}}/I_{15\text{ K}}$) is about three times higher in the GaN NSs than in the GaN epilayer. This fact reflects a better internal quantum efficiency of the GaN NSs due to the improved crystal quality by the removal of defects. We also measured the low-temperature micro-PL with high spatial and spectral resolutions to observe a small number

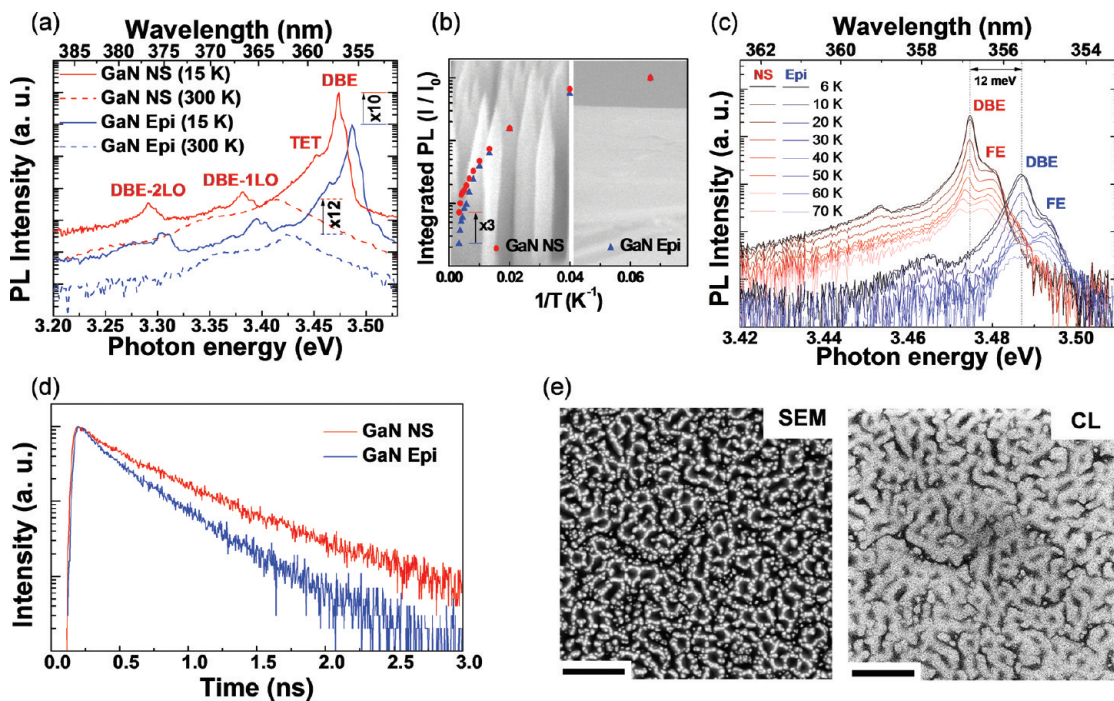


Figure 4. Comparison of optical properties of the GaN NSs and the GaN epilayer. (a) PL spectra (log scale) of the GaN NSs (red line) and the GaN epilayer (blue line) at 15 K (solid line) and at 300 K (dash line). The positions of the DBE, the two electron transition (TET) of the DBE and the longitudinal optical (LO) phonon replicas are marked. (b) An Arrhenius plot of the normalized integrated PL intensity (log scale) of the GaN NSs (red circle) and the GaN epilayer (blue triangle). The background shows bird's eye-view SEM images of the GaN NSs (left) and the GaN epilayer (right). (c) Micro-PL spectra (log scale) of the GaN NSs (red lines) and the GaN epilayer (blue lines) for various low temperatures. (d) Time-resolved PL spectra of the GaN NSs (red line) and the GaN epilayer (blue line) measured at 300 K. (e) Plan-view SEM and monochromatic (364 nm) CL images of the GaN NSs taken at the same position and room temperature. The bright regions in the SEM image and the CL image indicate the GaN NSs and near-band-emission, respectively. Scale bars = 1 μ m.

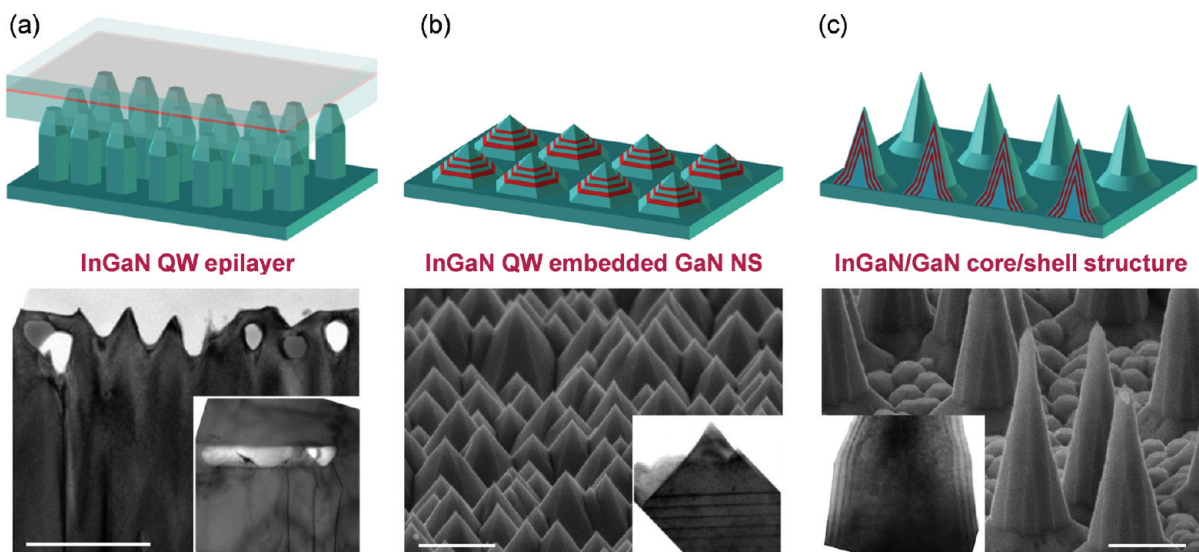


Figure 5. Fabrication of various series of InGaN QW structures. (a) Formation of high-quality InGaN QW layers on etched GaN NSs. Lower panel shows the cross-sectional TEM image for the initial stage of regrowth process. After the finish of regrowth process, dislocation blocking by the voids is shown in the inset TEM image. (b) Formation of InGaN QW embedded nanopyramid structure. Bird's eye-view SEM image shows high-quality and high-density nanopyramids on a large area by the CVE method. Inset: cross-sectional TEM image for InGaN QW embedded nanopyramid. (c) InGaN/GaN core/shell structures were formed by regrowing InGaN QW on etched GaN NSs. Bird's eye-view SEM image shows dodecahedral nanopyramids with highly inclined facets. Inset: cross-sectional TEM image for InGaN/GaN core/shell structure. Scale bars = 500 nm.

of NSs instead of large ensembles of NSs and to clarify the peak positions of the donor-bound exciton (DBE) and the free exciton (FE) (Figure 4c). As with the macro-PL results above, we observed that the peak intensity of the GaN NSs was

enhanced by more than 1 order of magnitude with a red shift of 12 meV. A comparison of the fwhm in the DBE peak at 6 K reveals that the fwhm is 1.9 meV for the GaN NSs and 2.5 meV for the GaN epilayer. This narrowing of the fwhm reflects again

the improvement in the crystal quality of the GaN NSs.³¹ The improved crystal quality of the GaN NSs affects its recombination time. The time-resolved PL was measured at 15 and 300 K. At a low temperature, the GaN NSs and the GaN epilayer have a similar recombination time of 150 ps at the peak position (Figure S3 in the Supporting Information). However, the GaN NSs show a longer recombination time (380 ps) than that of the GaN epilayer (260 ps) at room temperature (Figure 4d). Generally, the nonradiative process becomes predominant at room temperature. Therefore, this result indicates that the nonradiative recombination time of the GaN NSs was prolonged compared with that of the GaN epilayer due to the reduction of defects in the GaN NSs. A monochromatic CL image of the GaN NSs was taken at a near-band-edge emission of 364 nm and room temperature (Figure 4e). By comparing the plan-view SEM and CL images of the GaN NSs taken at the same position, we observed that the near-band-edge emission of the GaN is mostly emitted from the high-quality NSs, not from the poor-quality etched-bottom region.

The light emitting efficiency of materials can be represented by the external quantum efficiency which is the product of the internal quantum efficiency and light extraction efficiency. We found that both the internal quantum efficiency and light extraction efficiency were improved in the GaN NSs formed by the CVE method. These superior optical properties of the GaN NSs correspond well with its structural characteristics: the good shape for light emission and strain relaxation as well as the removal of dislocations.

As an application of these chemically etched high-quality GaN NSs, we have designed and demonstrated various series of modified structures containing InGaN QW (Figure 5). First, we grew InGaN QW layers on as-etched GaN NSs using MOCVD (Figure 5a and Figure S4 in the Supporting Information). At the initial stage of regrowth process, lateral growth occurs at the top of NSs and bridges each NSs (lower in Figure 5a). This lateral growth process resulted in the formation of voids and high-quality InGaN QW layers were then grown on this void embedded GaN layer. Inset in Figure 5a shows that the voids play a role not only of strain reduction but of dislocation blocking. Comparing common lateral over growth techniques,³² our approach forms voids on dislocations and prevents the propagation of dislocations without any patterning work. Second, we fabricated InGaN QW embedded nanopyramid structures by the chemical etching of InGaN QW epilayer instead of GaN epilayer (Figure 5b and Figure S5 in the Supporting Information). High-density and high-quality InGaN QW embedded nanopyramid structures were formed on a large area. We can expect a large increase of light extraction and carrier localization in this nanopyramid structure. Third, we formed InGaN/GaN core/shell NSs by regrowing InGaN QW on etched GaN nanopyramid structure (Figure 5c and Figure S6 in the Supporting Information). To fabricate these structures, we used the etched GaN NSs with a larger size and lower density than the above two series. Therefore, the InGaN QW layer could successfully cover the whole surface of the GaN NSs, instead of forming a void. In this structure, we found a unique feature. The regrown InGaN NSs showed dodecagonal facets, while the as-etched GaN NS had hexagonal facets (Figure S6 in the Supporting Information). These InGaN/GaN core/shell NSs have an advantage of increased surface area of active layer as well as efficient light extraction. The above-mentioned various series of InGaN QW structures

using the CVE method showed the potential applicable structures toward high-efficiency and dislocation-free InGaN-based light emitting devices. Further details on these structures are left as future work.

CONCLUSION

We reported on chemically controlled GaN NSs and applications to various types of InGaN QW structures using the CVE method. In contrast with the common chemical etching method, the CVE method can effectively etch GaN and form dislocation-free GaN NSs with various shapes via the facet- and defect-selective dissociation processes. The as-etched GaN NSs showed improved crystal quality by the removal of dislocations and by the reduced residual strain and enhanced light extraction, resulting in excellent optical performances of the GaN NSs. To our knowledge, the CVE method is the first successful top-down chemical process for vertically aligned high-quality GaN NSs on a wafer level, and it also showed many possibilities of the fascinating applications for high-efficiency InGaN QW structures. We expect that the CVE method will serve as a new approach for chemical control of GaN and for the formation of nitride-based NSs.

ASSOCIATED CONTENT

Supporting Information

Additional SEM and TEM images of the GaN NSs and InGaN quantum well structures and carrier recombination property at various temperature and excitation power. This material is available free of charge via the Internet at <http://pubs.acs.org>.

AUTHOR INFORMATION

Corresponding Author

*Phone: +82-42-350-2549. Fax: +82-42-350-5549. E-mail: yhc@kaist.ac.kr.

ACKNOWLEDGMENTS

This work was supported by the WCU Program (No. R31-2008-000-1071-0) of the Ministry of Education, Science and Technology and the KAIST EEMS Initiative.

REFERENCES

- (1) Nakamura, S.; Mukai, T.; Senoh, M. *Appl. Phys. Lett.* **1994**, *64*, 1687–1689.
- (2) Nakamura, S.; Fasol, G.; Pearton, S. J. *The Blue Laser Diode: The Complete Story*; Springer: Berlin, 2000.
- (3) Razeghi, M.; Henini, M. *Optoelectronic Devices: III-nitrides 1–9*; Elsevier Science Ltd: Amsterdam, 2004.
- (4) Morkoc, H.; Mohammad, S. N. *Science* **1995**, *267*, 51–55.
- (5) Johnson, J. C.; Choi, H. J.; Knutson, K. P.; Schaller, R. D.; Yang, P.; Saykally, R. J. *Nat. Mater.* **2002**, *1*, 106–109.
- (6) Zang, K.; Chua, S. J. *Phys. Status Solidi C* **2010**, *7*, 2236–2239.
- (7) Kim, H. M.; Cho, Y. H.; Lee, H.; Kim, S. I.; Ryu, S. R.; Kim, D. Y.; Kang, T. W.; Chung, K. S. *Nano Lett.* **2004**, *4*, 1059–1062.
- (8) Park, Y. S.; Lee, S. H.; Oh, J. E.; Park, C. M.; Kang, T. W. *J. Cryst. Growth* **2005**, *282*, 313–319.
- (9) Hersee, S. D.; Sun, X.; Wang, X. *Nano Lett.* **2006**, *6*, 1808–1811.
- (10) Kuykendall, T.; Pauzauskie, P. J.; Zhang, Y.; Goldberger, J.; Sirbuly, D.; Denlinger, J.; Yang, P. *Nat. Mater.* **2004**, *3*, 524–528.
- (11) Hahn, Y. B.; Choi, R. J.; Hong, J. H.; Park, H. J.; Choi, C. S.; Lee, H. J. *J. Appl. Phys.* **2002**, *92*, 1189–1194.
- (12) Hennessy, K.; Badolato, A.; Tamboli, A.; Petroff, P. M.; Hu, E.; Atatüre, M.; Dreiser, J.; Imamoglu, A. *Appl. Phys. Lett.* **2005**, *87*, 021108.

- (13) Vartuli, C. B.; Pearton, S. J.; Abernathy, C. R.; Mackenzie, J. D.; Ren, F.; Zolper, J. C.; Shul, R. J. *Solid-State Electron* **1997**, *41*, 1947–1951.
- (14) Weyher, J. L.; Brown, P. D.; Rouviere, J. L.; Wosinski, T.; Zauner, A. R. A.; Grzegory, I. *J. Cryst. Growth* **2000**, *210*, 151–156.
- (15) Hino, T.; Tomiya, S.; Miyajima, T.; Yanashima, K.; Hashimoto, S.; Ikeda, M. *Appl. Phys. Lett.* **2000**, *76*, 3421–3423.
- (16) Ng, H. M.; Parz, W.; Weinmann, N. G.; Chowdhury, A. *Jpn. J. Appl. Phys.* **2003**, *42*, L1405–L1407.
- (17) Mastro, M. A.; Kryliouk, O. M.; Reed, M. D.; Anderson, T. J.; Davydov, A.; Shapiro, A. *Phys. Status Solidi A* **2001**, *188*, 467–471.
- (18) Aujol, E.; Napierala, J.; Trassoudaine, A.; Gil-Lafon, E.; Cadoret, R. *J. Cryst. Growth* **2001**, *222*, 538–548.
- (19) Akasaka, T.; Kobayashi, Y.; Ando, S.; Kobayashi, N.; Kumagai, M. *J. Cryst. Growth* **1998**, *260*, 72–77.
- (20) Miyake, H.; Motogaito, A.; Hiramatsu, K. *Jpn. J. Appl. Phys.* **1999**, *38*, L1000–L1002.
- (21) Claudon, J.; Bleuse, J.; Malik, N. S.; Bazin, M.; Jaffrennou, P.; Gregersen, N.; Sauvan, C.; Lalanne, P.; Gerard, J. M. *Nat. Photonics* **2010**, *4*, 174–177.
- (22) Lee, C. J.; Lee, T. J.; Lyu, S. C.; Zhang, Y.; Ruh, H.; Lee, H. J. *Appl. Phys. Lett.* **2002**, *81*, 3648–3650.
- (23) Liu, H. P.; Tsay, J. D.; Liu, W. Y.; Guo, Y. D.; Hsu, J. T.; Chen, I. G. *J. Cryst. Growth* **2004**, *260*, 79–84.
- (24) Du, D.; Srolovitz, D. J.; Coltrin, M. E.; Mitchell, C. C. *Phys. Rev. Lett.* **2005**, *95*, 155503.
- (25) Jindal, V.; Shahedipour-Sandvik, F. *J. Appl. Phys.* **2009**, *106*, 083115.
- (26) Sun, Q.; Yerino, C. D.; Ko, T. S.; Cho, Y. S.; Lee, I. H.; Han, J.; Coltrin, M. E. *J. Appl. Phys.* **2008**, *109*, 093523.
- (27) Shahedipour-Sandvik, F.; Grandusky, J.; Alizadeh, A.; Keimel, C.; Ganti, S. P.; Taylor, S. T.; LeBoeuf, S. F.; Sharma, P. *Appl. Phys. Lett.* **2005**, *87*, 233108.
- (28) Kisielowski, C.; Kruger, J.; Ruvimov, S.; Suski, T.; Ager, J. W. III; Jones, E.; Lilienthal-Weber, Z.; Rubin, M.; Weber, E. R.; Bremser, M. D.; Davis, R. F. *Phys. Rev. B* **1996**, *54*, 17745–17753.
- (29) Shan, W.; Fischer, A. J.; Hwang, S. J.; Little, B. D.; Hauenstein, R. J.; Xie, X. C.; Song, J. J.; Kim, D. S.; Goldenberg, B.; Horning, R.; Krishnankutty, S.; Perry, W. G.; Bremser, M. D.; Davis, R. F. *J. Appl. Phys.* **1998**, *83*, 455–461.
- (30) Li, Q.; Lin, Y.; Creighton, J. R.; Figiel, J. J.; Wang, G. T. *Adv. Mater.* **2009**, *21*, 2416–2420.
- (31) Yamada, T.; Yamane, H.; Goto, T.; Yao, T.; Yao, Y.; Sekiguchi, T. *Cryst. Res. Technol.* **2007**, *42*, 713–717.
- (32) Nam, O. H.; Bremser, M. D.; Zheleva, T. S.; Davis, R. F. *Appl. Phys. Lett.* **1997**, *71*, 2638–2640.